ARMY RESEARCH LABORATORY

Classical Dynamics Simulations of Unimolecular Decomposition of CH_2NNO_2: HONO Elimination vs. N–N Bond Scission

Betsy M. Rice
U.S. ARMY RESEARCH LABORATORY

Donald L. Thompson
OKLAHOMA STATE UNIVERSITY

ARL-TR-691 February 1995

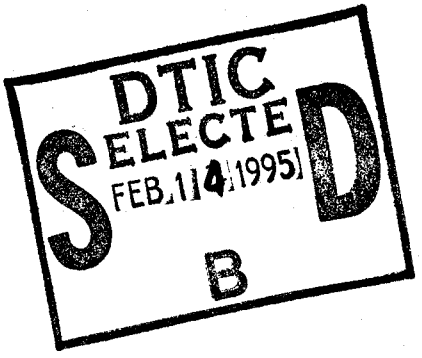

APPROVED FOR PUBLIC RELEASE; DISTRIBUTION IS UNLIMITED.

19950207 005

NOTICES

Destroy this report when it is no longer needed. DO NOT return it to the originator.

Additional copies of this report may be obtained from the National Technical Information Service, U.S. Department of Commerce, 5285 Port Royal Road, Springfield, VA 22161.

The findings of this report are not to be construed as an official Department of the Army position, unless so designated by other authorized documents.

The use of trade names or manufacturers' names in this report does not constitute endorsement of any commercial product.

REPORT DOCUMENTATION PAGE

Form Approved
OMB No. 0704-0188

Public reporting burden for this collection of information is estimated to average 1 hour per response, including the time for reviewing instructions, searching existing data sources, gathering and maintaining the data needed, and completing and reviewing the collection of information. Send comments regarding this burden estimate or any other aspect of this collection of information, including suggestions for reducing this burden, to Washington Headquarters Services, Directorate for Information Operations and Reports, 1215 Jefferson Davis Highway, Suite 1204, Arlington, VA 22202-4302, and to the Office of Management and Budget, Paperwork Reduction Project (0704-0188), Washington, DC 20503.

1. AGENCY USE ONLY (Leave blank)	2. REPORT DATE	3. REPORT TYPE AND DATES COVERED
	February 1995	Final, September 1993–June 1994

4. TITLE AND SUBTITLE

Classical Dynamics Simulations of Unimolecular Decomposition of CH_2NNO_2: HONO Elimination vs. N–N Bond Scission

5. FUNDING NUMBERS

PR: 1L161102AH43

6. AUTHOR(S)

Betsy M. Rice and Donald L. Thompson*

7. PERFORMING ORGANIZATION NAME(S) AND ADDRESS(ES)

U.S. Army Research Laboratory
ATTN: AMSRL-WT-PC
Aberdeen Proving Ground, MD 21005-5066

8. PERFORMING ORGANIZATION REPORT NUMBER

9. SPONSORING / MONITORING AGENCY NAME(S) AND ADDRESS(ES)

U.S. Army Research Laboratory
ATTN: AMSRL-OP-AP-L
Aberdeen Proving Ground, MD 21005-5066

10. SPONSORING / MONITORING AGENCY REPORT NUMBER

ARL-TR-691

11. SUPPLEMENTARY NOTES

* Professor Thompson is employed by Oklahoma State University.

12a. DISTRIBUTION / AVAILABILITY STATEMENT

Approved for public release; distribution is unlimited.

12b. DISTRIBUTION CODE

13. ABSTRACT *(Maximum 200 words)*

Classical dynamics simulations of the unimolecular decomposition of CH_2NNO_2 have been performed. The potential energy function was based on MCSCF and MRCI calculations of Mowrey et al. (1990). CH_2NNO_2 primary decomposition rates and mechanisms are presented. The two primary decomposition pathways are (I) N-N bond scission to form H_2CN and NO_2 and (II) concerted dissociation via a five-center transition state to eliminate HONO + HCN. The classical barrier heights differ by 2 kcal/mol. Reactions (I) and (II) are first-order decay processes and are well-behaved with increasing energy. At low energies, (I) is the major decomposition pathway, but at high energies, (II) becomes equally probable. Product energy distributions for (I) are unremarkable, with the relative translational and rotational distributions peaked near zero; however, distributions for (II) show interesting behavior. The trajectories resulting in (II) that do not experience secondary HONO decomposition have a translational energy distribution shifting significantly away from zero, as expected with large back reaction barriers. The trajectories resulting in (II) that undergo secondary HONO decomposition, however, have a distribution that is similar to the distributions in (I), indicating little translational energy excitation upon formation. Rotational energy distributions for (II) are peaked near zero, regardless of whether HONO decomposes. Most of the available product energy for (II) goes into vibration. Our results, calculated under microcanonical conditions in which energy is partitioned in a statistical manner among the internal modes, are not consistent with the RDX molecular beam measurements in which CH_2NNO_2 is a primary decomposition product which decomposes only through concerted molecular eliminations.

14. SUBJECT TERMS

decomposition, unimolecular decomposition, methylene nitramine, molecular dynamics

15. NUMBER OF PAGES

24

16. PRICE CODE

17. SECURITY CLASSIFICATION OF REPORT	18. SECURITY CLASSIFICATION OF THIS PAGE	19. SECURITY CLASSIFICATION OF ABSTRACT	20. LIMITATION OF ABSTRACT
UNCLASSIFIED	UNCLASSIFIED	UNCLASSIFIED	UL

INTENTIONALLY LEFT BLANK.

ACKNOWLEDGMENTS

Professor Thompson gratefully acknowledges support from the U.S. Army Research Office. Some of the calculations were performed at the Department of Defense (DOD) High-Performance Computing Center (HPC) at Corps of Engineers Waterways Experimental Station (CEWES), Vicksburg, MS.

Accession For
NTIS GRA&I ☑
DTIC TAB ☐
Unannounced ☐
Justification
By
Distribution
Availability Codes
Dist | Avail and/or Special
A-1

INTENTIONALLY LEFT BLANK.

TABLE OF CONTENTS

INTENTIONALLY LEFT BLANK.

LIST OF FIGURES

INTENTIONALLY LEFT BLANK.

LIST OF TABLES

INTENTIONALLY LEFT BLANK.

1. INTRODUCTION

The work presented here is a continuation of attempts to unravel details of reactions that occur in the decomposition of hexahydro-1,3,5-trinitro-1,3,5-triazine, more commonly known as RDX. The primary decomposition of this nitramine under collisionless, infrared multiphoton excitation (IRMPE) conditions occurs through two competing reactions (Zhao, Hintsa, and Lee 1988), denoted (P1) and (P2) below. The reactions are scission of the weakest bond ($N–NO_2$) to form an unstable cyclic radical and NO_2:

$$RDX \rightarrow C_2H_4N_4O_4 + NO_2 \qquad (P1)$$

and concerted decomposition of the ring to form three highly vibrationally excited methylene nitramine (MN) molecules:

$$RDX \rightarrow 3\,CH_2NNO_2. \qquad (P2)$$

These reactions were determined by analyzing time-of-flight (TOF) mass spectra of products, and comparing these with predictions based on several proposed decomposition schemes (Zhao, Hintsa, and Lee 1988). Reactions that could not explain various components of the TOF spectra were then eliminated from the series of proposed reactions. In the case of the primary decomposition of RDX, reactions (P1) and (P2) were the two reactions that were consistent with the experimental measurements, particularly concerning the TOF spectra of the large mass products (m/e > 74). However, a series of secondary decomposition reactions of RDX had to be invoked to fit all of the observed TOF spectra (Zhao, Hintsa, and Lee 1988).

The secondary reactions of (P2) proposed by Zhao, Hintsa, and Lee (1988) are all concerted molecular eliminations. They did not observe evidence of the simple scission reaction of the weakest bond in MN:

$$CH_2NNO_2 \rightarrow H_2CN + NO_2. \qquad (I)$$

They propose two channels for the decomposition of MN (Zhao, Hintsa, and Lee 1988):

$$CH_2NNO_2 \rightarrow HCN + HONO \text{ (or } HNO_2) \qquad (II)$$

and

$$CH_2NNO_2 \rightarrow N_2O + H_2CO. \qquad \text{(III)}$$

The TOF spectra indicate that (III) is a minor channel compared to the decomposition of MN through (II). The results of the experiments did not determine whether HONO or HNO_2 is the more probable isomer of (II).

There have been suggestions that the cyclic radical $C_2H_4N_4O_4$ of (P1) spontaneously decomposes to form MN (Schroeder 1985a; 1985b). Regardless of the parentage of MN, the determination of its fate is important in understanding RDX decomposition. The purpose of this study is to examine, by using classical trajectories, the reactions of highly-excited CH_2NNO_2, which may be a product of RDX decomposition. Unfortunately, the experimental measurements do not provide detailed information about the internal energy distributions of the nascent CH_2NNO_2. For example, it is not known whether the energy is distributed statistically. Zhao, Hintsa, and Lee (1988) estimate that the average internal energy of the RDX following IRMPE is approximately 80 kcal/mol. This information, in conjunction with a Hess' law analysis of the endothermicity of (P2) provided by Sewell and Thompson (1991), suggests that the MN molecules formed from (P2) have total energies ranging from 55–65 kcal/mol. This is sufficient energy for MN to undergo the decomposition reactions (I)–(III). Classical simulations of the primary decomposition of RDX (Sewell and Thompson 1991) show that most of the energy in the nascent CH_2NNO_2 is vibrational.

Methylene nitramine has never been isolated. The only characterizations of this molecule come from theoretical predictions. In a previous report, we developed a potential energy function of this molecule (Rice et al., submitted for publication). We based the potential energy surface (PES) of MN that we used in this work on the ab initio multiconfigurational (MC) SCF and multireference (MR) CI electronic structure calculations of Mowrey et al. (1990; unpublished). They calculated the structure, relative energies, and frequencies of equilibrium MN, the five-centered transition state for HONO elimination, and the asymptotes for the N–N scission reaction (Mowrey et al. 1990). Additionally, they calculated points along the reaction path from the five-centered transition state of (II) leading to reactants (MN) and products (HONO + HCN) (Mowrey et al. unpublished). After adjusting for zero-point energy effects, basis sets and different levels of theory, they estimate that the activation energy for (II) is 31 ± 4 kcal/mol. They also estimate the N–N bond dissociation energy for (I) to be 35 ± 4 kcal/mol. Although these estimates suggest that reaction (II) is energetically favored, the steric effects associated with reaction (II) would make reaction (I) entropically favored.

Mowrey et al. (1990) suggested that because Zhao, Hintsa, and Lee (1988) did not observe evidence of reaction (I), either (a) the microcanonical rate constant for (I) has an anomalous energy dependence which makes it not probable, or (b) the barrier height for (II) is substantially lower than (I) and the nascent MN do not have enough energy for (I) to occur. Mowrey et al. (1990) have investigated the latter and have shown that the activation energy for (II) is lower than, or at least comparable with, the N–N bond dissociation energy. In the present study, we have used detailed dynamical modeling to investigate whether MN exhibits an anomalous energy dependence of the decomposition rates. We have calculated the microcanonical rate constants for reactions (I) and (II) as functions of energy by using classical trajectories computed on an analytical PES that is based on the Mowrey et al. ab initio results (1990; unpublished). Additionally, mechanistic details of the reactions are presented.

2. POTENTIAL ENERGY SURFACE

The analytic PES that we used in this study is described in (Rice et al., submitted for publication). Structures corresponding to the reactant and transition state agree with the ab initio values (Mowrey et al. 1990) to within 0.5%. The normal modes of vibration for MN are in good agreement with the ab initio calculations (Mowrey et al. 1990). Also, the analytic function (Rice et al., submitted for publication) was fitted to points along the reaction path leading to products for (II) and are in good agreement with the ab initio values (Mowrey et al. 1990). The model PES predicts an activation energy for (II) of 31.8 kcal/mol, and the dissociation energy of the N–N bond is 35 kcal/mol (Rice et al., submitted for publication), in agreement with the Mowrey et al. estimates (1990).

3. METHODS

Trajectories at six energies were integrated using a variable-step Adams-Moulton predictor-corrector integrator (Miller and George 1972), with relative error tolerance set to 10^{-7}. Initial conditions were selected as follows: The molecule was initially in the equilibrium geometry. The total energy of the system, including the zero-point energy, was equipartitioned among the normal modes in the form of kinetic energy. A warmup trajectory of approximately 0.2 ps was integrated, allowing a partial repartitioning between potential and kinetic energy. These points in phase space were then used as starting points for Metropolis Monte Carlo sampling (Metropolis et al. 1953; Raff and Thompson 1985). An initial markov walk of 10^6 steps was taken to ensure that the system was relaxed away from the initial configuration. A trajectory was then integrated until the end tests indicated a reaction had occurred, or

until the simulation time exceeded 20 ps. A sequence of 4,000 markov moves was taken from the starting point of the previous trajectory, and the integration/markov walk pattern was repeated until an ensemble of at least 2,000 trajectories was generated. Three heavy atoms and one hydrogen atom were moved for each markov step. Step sizes for the markov walk (given in Table 1) were selected to achieve 50% acceptance of the attempted moves. Additionally, the maximum bond extensions were limited in the Metropolis sampling to confine the sampling to reactant configuration space. The N–N and C–H bonds were limited to less than 2.0 and 1.2 Å, respectively, and the H–O bond is restricted to be greater than 1.6 Å.

Table 1. Parameters Used in Metropolis Sampling

Atom Type	Maximum Coordinate Displacement (Å)	Maximum Momentum Change (amu-Å/t.u.[a])
H	0.035	0.025
C	0.028	0.025
N	0.025	0.028
O	0.025	0.035

[a] 1 t.u. = 1.018066×10^{-14} s.

The end tests used to identify the reaction type are listed in Table 2. There is sufficient energy in these simulations to allow for secondary reactions following the primary reactions (I) and (II). The secondary reactions observed in the simulations result from decomposition or isomerizations of the nascent HONO:

$$HONO' \rightarrow HO + NO' \qquad \text{(NO bond scission)} \qquad \text{(III)}$$

$$HONO' \rightarrow ONO'H \qquad \text{(Hydrogen Atom Migration)} \qquad \text{(IV)}$$

$$HONO' \rightarrow ONO' + H \qquad \text{(Hydrogen Atom Elimination)} \qquad \text{(V)}$$

For purposes of discussion, the two identical oxygen atoms listed in (III)–(V) are distinguished as O and O′. We will use these same distinctions later in the discussion of the results. If a trajectory triggers the end tests specifying HONO + HCN formation, ends tests for the secondary reactions are invoked. At this

Table 2. End Tests

Primary Decomposition Reactions:
$CH_2NNO_2 \rightarrow H_2CN + NO_2$
• $R_{NN} > 5.0$ Å, $R_{CH(1)} < 2.0$ Å, $R_{CH(2)} < 2.0$ Å
$CH_2NNO_2 \rightarrow HONO' + 'HCN$
• $R_{CH} > 2.0$ Å, $R_{OH} < 1.393$ Å, $R_{CH'} < 2.0$ Å and D_{NN}, $D_{CH} < 10^{-4}$ eV
Secondary Decomposition/Isomerization Reactions:
$HONO' \rightarrow H + ONO'$
• $R_{HO} > 5.0$ Å
$HONO' \rightarrow ONO'H$
• $R_{HO} > R_{HO'}$
$HONO' \rightarrow HO + NO'$
• $R_{NO} > 5.0$ Å, $R_{NO'} < 2.0$ Å

point in the trajectory calculation, the integration continues up to the maximum integration time (20 ps), or until the O–H or N–O bond distances exceed 5.0 Å.

The lifetime of a trajectory resulting in (I) was taken to be the integration time up to the last inner turning point of the N–N bond vibration. The lifetime of a trajectory resulting in (II) was taken to be the integration time up to the point at which all end tests for reaction (II) were satisfied.

4. RESULTS AND DISCUSSION

Table 3 is a summary of trajectory results for total energies (including the zero-point energy, 27.5 kcal/mol) ranging from 62 to 131 kcal/mol. At least 2,000 trajectories, including those recounted according to standard Metropolis sampling procedures (Metropolis et al. 1953; Raff and Thompson 1985),

Table 3. Ensemble Results

Primary Decomposition Reactions				
Energy[a] (kcal/mol)	Total Trajectories	Total Reactions[b]	Reaction I[c]	Reaction II[c]
62.1	4635	364 (8)	322 (88)	42 (12)
73.6	1997	787 (39)	673 (86)	114 (14)
85.1	1995	1646 (82)	1274 (77)	372 (23)
96.7	2001	1968 (98)	1523 (77)	445 (23)
108.2	1963	1963 (100)	1340 (68)	623 (32)
119.7	1946	1946 (100)	1199 (62)	747 (38)
131.3	1938	1938 (100)	1145 (59)	793 (41)
Secondary Decomposition Reactions of HONO				
Energy[a] (kcal/mol)	Unreacted[d] HONO+HCN	HO+NO+HCN[d]	H+ONO+HCN[d]	H-Atom Migration in HONO
62.1	42 (100)	0 (0)	0	4
73.6	114 (100)	0 (0)	0	2
85.1	363 (98)	9 (2)	0	10
96.7	421 (94)	24 (6)	0	10
108.2	585 (94)	38 (6)	0	27
119.7	663 (89)	84 (11)	0	84
131.3	654 (82)	130 (16)	9 (1)	118

[a] Includes the zero-point energy.
[b] Values in parentheses are percentage of trajectories resulting in reaction.
[c] Values in parentheses are percentage of the total reactions.
[d] Values in parentheses are percentages of reaction II totals.

were used in ensemble averaging for each energy. Because of the low number of reactions at 62.1 kcal/mol, approximately 4,600 trajectories were calculated to attain better statistics. Trajectories that satisfied the end tests for N–N bond scission, but had not undergone at least one N–N vibration were not included in the ensemble averages or reaction totals. The number of these rejected trajectories increased with increasing energy, leading to the fewer trajectories available for averaging at the higher energies.

The numbers in parentheses in the column entitled "Total Reactions" are the percentages of CH_2NNO_2 that react within the integration time of 20 ps. At energies greater than 97 kcal/mol, every trajectory results in reaction within this time.

Table 3 also lists the numbers of trajectories (and reaction percentages in parentheses) resulting in reactions (I) or (II). The majority of reacting trajectories over the energies sampled result in reaction (I), but this majority decreases at higher energies as reaction (II) becomes more probable. Additionally, there is an increase in the secondary N–O scission and H-atom migration reactions of HONO as energy increases. The increase in both of these secondary reactions as the total energy increases is not surprising. The increase in the secondary reactions of HONO is probably due not only to the details of HONO formation, but also on the internal energy distribution of the CH_2NNO_2 before reaction. As the total internal energy of CH_2NNO_2 increases, the energy distributed among the internal modes increases, including the vibrational modes corresponding to the ONO moiety. Upon reaction, additional energy is released to the fragments. Because the ONO moiety does not undergo bond breaking or significant geometric change in the transformation from CH_2NNO_2 to HONO, it is reasonable to assume that the ONO moiety maintains (or even gains) vibrational excitation, some of which result in the secondary reactions corresponding to either N–O bond scission, or the large-amplitude bending motion of HONO to accomplish H-atom migration.

We did not observe enough secondary HONO decomposition reactions resulting in H + ONO to determine the energy dependence of this channel. We observed these reactions only at one energy, and the mechanism appears to be the same for each event. The mechanism is illustrated in Figure 1. Figure 1 shows the behavior of the N–O, N=O′, and H–O distances during one of the trajectories that results in H-atom elimination from HONO. In this trajectory, HONO′ + HCN forms within 0.1 ps. Upon formation of HONO, the nascent H–O bond is highly vibrationally excited. The energy localized in this bond transfers to the remaining vibrational modes, including the adjacent N–O bond. The N–O bond appears to experience increasing excitation up to 3.0 ps, evident by the large-amplitude motion. At this time, the energy appears to flow out of the N–O bond and back into the adjacent H–O bond, also evident by the large-amplitude oscillations of this bond at times greater than 3.0 ps. At 3.75 ps, enough energy has transferred back into the H–O bond to cause dissociation to H + ONO′. Throughout the trajectory, the terminal N=O′ bond does not experience significant vibrational excitation.

A more typical trajectory resulting in secondary decomposition of HONO to diatomic products is illustrated in Figure 2. This trajectory also shows a hydrogen migration reaction in the HONO before the decomposition event. At approximately 0.6 ps, CH_2NNO_2 form HO′NO + HCN, which is most evident by the behavior of the H–O′ bond in Figure 2d. After approximately 1 ps, the hydrogen migrates on the HO′NO molecule to form HONO′. After another 4 ps, the N–O bond breaks and the diatomics HO + NO′ are formed.

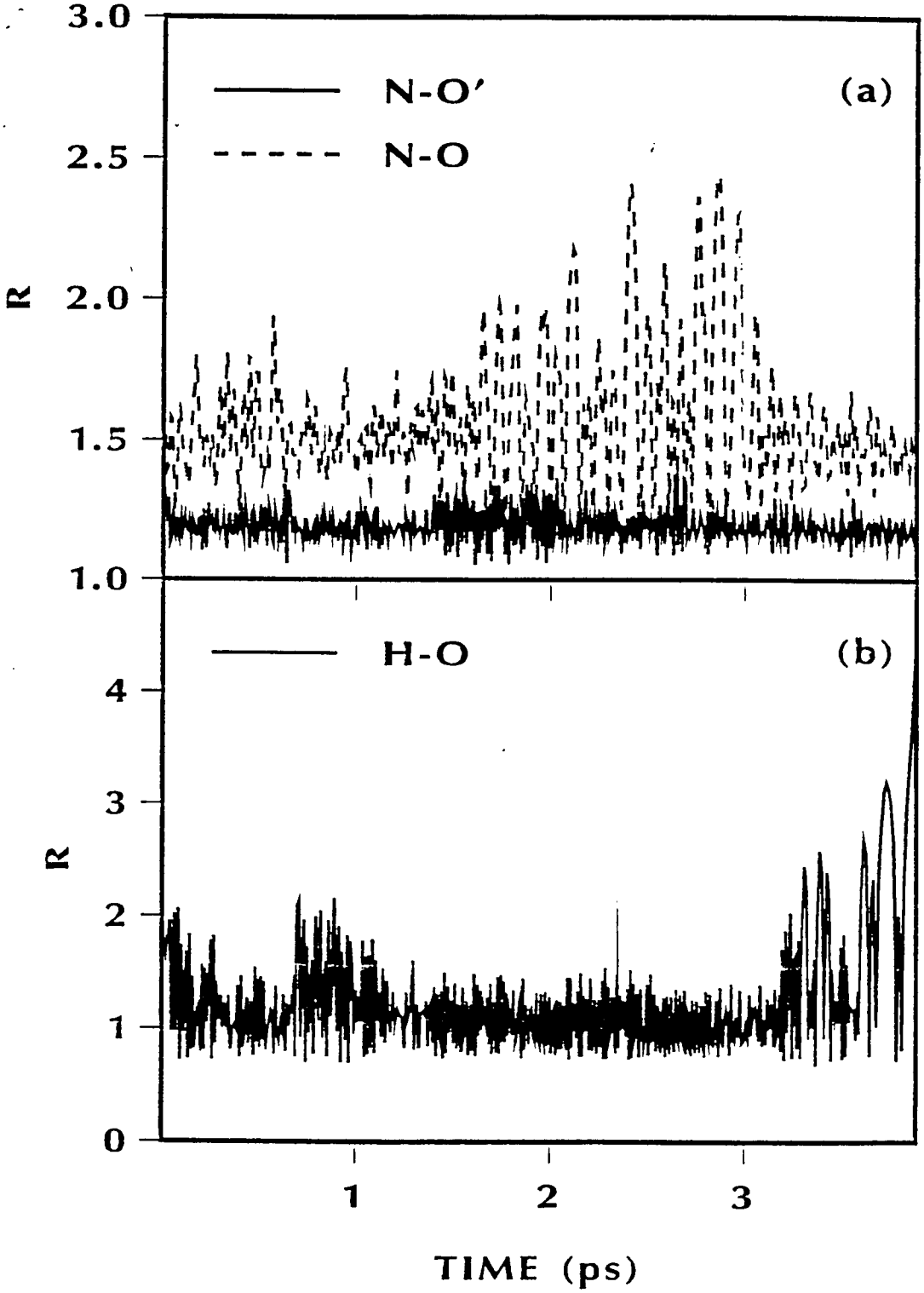

Figure 1. Internal coordinates (a) N–O and N–O′ and (b) H–O in HONO′ formed from primary decomposition of CH_2NNO_2 during a trajectory that results in secondary H–O bond scission of the HONO′ molecule.

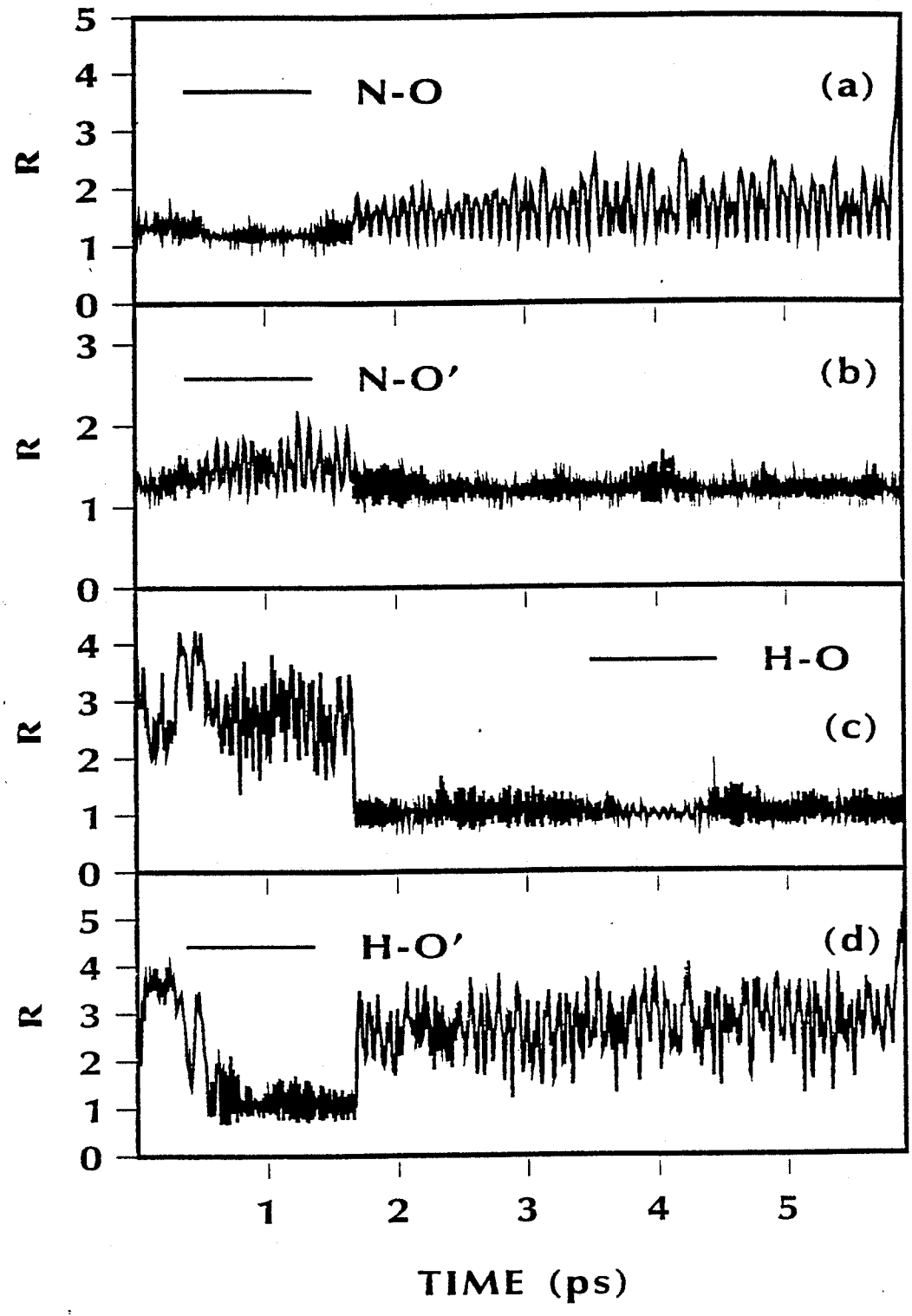

Figure 2. Internal coordinates (a) N–O, (b) N–O′, (c) H–O, and (d) H–O′ in HO′NO formed from primary decomposition of CH_2NNO_2 during a trajectory that results in hydrogen migration followed by N–O′ scission of the HO′NO molecule.

Table 4 lists the decay coefficients and branching ratios for the primary decomposition reactions of CH_2NNO_2 as functions of energy. For a system of molecules undergoing unimolecular decomposition through two competing channels, the overall rate of decomposition can be expressed as:

$$k_{Total} = k_I + k_{II} \tag{1}$$

and can be determined from trajectory results by fitting lifetimes to:

$$\ln[P] = -k_{Total}t\ , \tag{2}$$

where [P] is the fraction of unreacted CH_2NNO_2 at time t. The individual rate coefficients, k_I and k_{II}, can be extracted from the branching ratio (defined in this calculation as the ratio N_I/N_{II}, the total number of N–N bond scission reactions to the total number of HONO formations) using the following relation:

$$N_I/N_{II} = k_I/k_{II}\ . \tag{3}$$

The decay curves and corresponding branching ratios are shown in Figure 3. All of the decay curves and branching ratios are linear, indicating that the rate for this system is first-order and time independent. Linear least-squares fits of Equations (2) and (3) to these curves resulted in the rate coefficients listed in Table 4.

We have also fitted the total decay rate and individual rates as a function of energy to the RRK statistical model (Robinson and Holbrook 1972)

$$k(E) = \nu\left(\frac{E - E_0}{E}\right)^{(s-1)}\ , \tag{4}$$

where E_0 is set to 35 kcal/mol.

The results of the fit to the three rate coefficients, k_{Total}, k_I, and k_{II}, as a function of energy are shown in Figures 4a and 4b. Values of the best-fit parameters are given in Table 4. Because this system is so well-behaved and k_{Total}, k_I, and k_{II} are well-described by the RRK model, we were able to obtain a functional description of the branching ratios

$$\frac{N_I}{N_{II}}(E) = \frac{\nu_I}{\nu_{II}}\left(\frac{E - E_0}{E}\right)^{(s_I - s_{II})} . \qquad (5)$$

The branching ratios and prediction using the RRK parameters provided in Table 4 are shown in Figure 4c. If the behavior of this system can be well-described by this model for energies much greater than those sampled, then the limit at high energy of the branching ratio is 0.47, indicating that most of the high-energy reactions are concerted. The results indicate that the microcanonical reaction rates have no anomalous energy dependence and are very well-behaved. This system does not exhibit nonstatistical behavior for microcanonical initial conditions, which ensures a statistical distribution of total energy among the internal modes of the molecule.

Table 4. Decay Coefficients and Branching Ratios

Energy[a]	k_{Total} (ps^{-1})	k_I (ps^{-1})	k_{II} (ps^{-1})	k_I/k_{II}
62.1	0.004	0.0036	0.00037	9.6
73.6	0.024	0.021	0.0036	5.7
85.1	0.089	0.070	0.019	3.7
96.7	0.23	0.18	0.053	3.4
108.2	0.40	0.27	0.13	2.1
119.7	0.68	0.42	0.26	1.6
131.3	1.07	0.61	0.46	1.3
ν (ps^{-1})	42.9326	13.7587	29.1739	—
s	12.915	10.9636	14.6706	—

Table 5 lists the average product translational and rotational energies for the various primary and secondary decomposition reactions of CH_2NNO_2. The numbers in parentheses are the percentages of energy available to the products in translation and rotation. For reaction (I), most (~60%) of the available energy is in vibration, with slightly more energy going into relative translation than into the rotational modes. The results listed for reaction (II) are compiled from those trajectories that did not undergo secondary decomposition of HONO. In contrast to reaction (I), approximately 1/3 of the available energy goes into relative translation. HCN experiences almost double the rotational excitation that HONO does, but these amounts are insignificant compared to the amount of energy deposited in the vibrational modes (~50%).

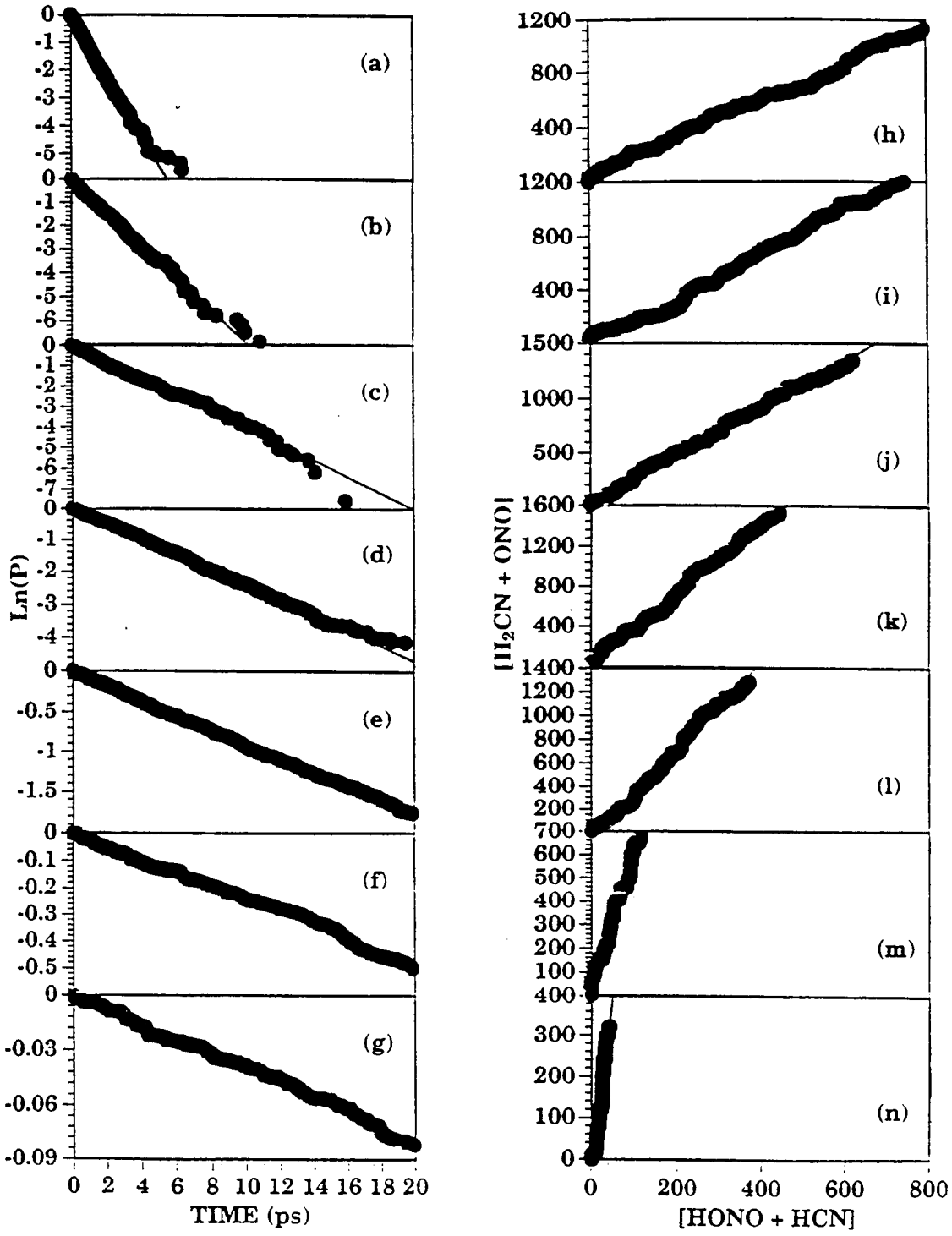

Figure 3. Unimolecular decay curves for the primary decomposition of CH_2NNO_2 at (a) 131.3 kcal/mol, (b) 119.7 kcal/mol, (c) 108.2 kcal/mol, (d) 96.7 kcal/mol, (e) 85.1 kcal/mol, (f) 73.6 kcal/mol, and (g) 62.1 kcal/mol. Figure (h)–(n) are the branching ratios corresponding to decay curves (a)–(g).

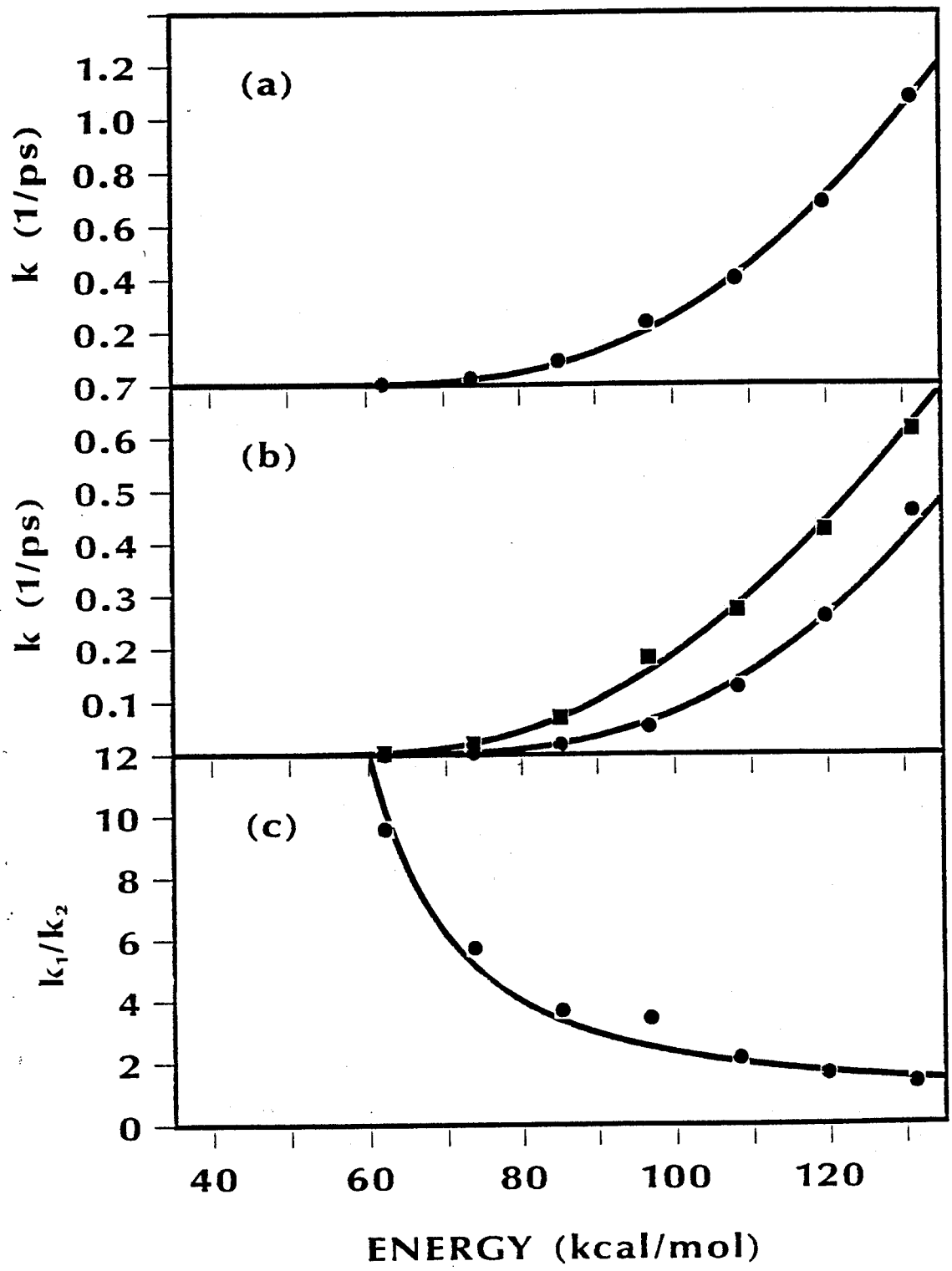

Figure 4. (a) k_{Total} and (b) k_I [squares] and k_{II} [circles] and (c) branching ratio as functions of energy. Points are trajectory results; the solid lines are RRK fits to the trajectory results.

Table 5. Product Energy Partitioning[a]

Reaction I: $CH_2NNO_2 \rightarrow H_2CH + ONO$				
Initial Energy[b]	Available Product Energy	$\langle E_{Trans} \rangle$	$\langle E_{Rot} \rangle$, H_2CH	$\langle E_{Rot} \rangle$, ONO
62.1	27.1	4.4 (16)	3.0 (11)	2.3 (8)
73.6	38.6	6.9 (18)	3.9 (10)	3.7 (10)
85.1	50.1	9.0 (18)	5.5 (11)	4.6 (9)
96.7	61.7	10.8 (18)	7.1 (12)	5.8 (9)
108.2	73.2	12.0 (16)	7.4 (10)	7.6 (10)
119.7	84.7	15.7 (18)	9.7 (12)	7.4 (9)
131.3	96.3	16.6 (17)	9.9 (10)	9.2 (10)
Reaction II: $CH_2NNO_2 \rightarrow$ HONO + HCN (no secondary reactions)				
Initial Energy[b]	Available Product Energy	$\langle E_{Trans} \rangle$	$\langle E_{Rot} \rangle$, HONO	$\langle E_{Rot} \rangle$, HCN
62.1	90.0	15.2 (17)	4.8 (5)	8.3 (9)
73.6	101.5	26.3 (26)	3.9 (4)	12.9 (13)
85.1	113.0	33.0 (29)	5.1 (4)	15.9 (14)
96.7	124.6	36.2 (29)	7.1 (6)	17.8 (14)
108.2	136.1	39.4 (29)	7.6 (6)	19.4 (14)
119.7	147.6	41.0 (28)	8.8 (6)	21.0 (14)
131.3	159.2	46.1 (29)	9.7 (6)	22.6 (14)

Reaction III: $CH_2NNO_2 \rightarrow$ HONO + HCN $\rightarrow$ HO + NO + HCN						
Initial Energy	Available Product Energy	$\langle E_{Trans} \rangle$,[c] (HO+NO) + HCN	$\langle E_{Rot} \rangle$,[c] HCN	$\langle E_{Trans} \rangle$,[d] HO+NO	$\langle E_{Rot} \rangle$,[d] HO	$\langle E_{Rot} \rangle$,[d] NO
62.1	38.0	—	—	—	—	—
73.6	49.5	—	—	—	—	—
85.1	61.0	5.3 (5)	11.8 (10)	19.4 (32)	1.5 (2)	3.0 (5)
96.7	72.6	9.2 (7)	2.8 (2)	26.1 (36)	3.2 (4)	7.6 (10)
108.2	84.1	12.0 (9)	7.1 (5)	29.1 (35)	6.2 (7)	5.8 (7)
119.7	95.6	11.8 (8)	11.1 (8)	27.0 (28)	5.5 (6)	11.1 (12)
131.3	107.2	12.5 (8)	13.1 (8)	30.4 (28)	5.5 (5)	7.8 (7.3)

[a] Energy given in kcal/mol.
[b] Includes the zero-point energy.
[c] Percentage of available product energy of unreacted HONO + HCN.
[d] Percentage of available product energy after HONO decomposition.

Average product energies for trajectories resulting in secondary decomposition of HONO are compared to those that do not undergo HONO decomposition in Table 5. The percentages of available product

energy in the columns labeled $<E_{Trans}>$, (HO+NO) + HCN and $<E_{Rot}>$, HCN in Table 5 are percentages of the available product energy upon HONO formation from CH_2NNO_2. These results are directly comparable to the average relative translational energy and average HCN rotational energies for the HONO trajectories that do not react. The rotational energy distributions of HCN do not differ significantly between the two subsets of trajectories. For the trajectories that result in secondary decomposition of HONO, the average HCN rotational energy is slightly less than that corresponding to unreacted HONO. The average relative translational energy distributions for trajectories resulting in secondary decomposition of HONO, however, differ substantially from those corresponding to unreacted HONO.

Figure 5 shows the relative translational energy distributions upon HONO formation for trajectories that do not undergo secondary decomposition (black filled bars) and those that do (grey-shaded bars) for 131 kcal/mol total energy. The distribution of the trajectories that result in secondary decomposition of HONO is peaked near 10 kcal/mol and has an average value corresponding to 8% of the available product energy. We estimate that as much as 75% of the energy available to products goes into the vibrational modes of the HONO that will subsequently decompose. The distribution corresponding to unreacted HONO peaks at 55 kcal/mol, and has an average value of 29% of the available product energy. We estimate that only 50% of the available product energy goes into vibration for this subset of trajectories resulting in HONO formation. It is clear that the destiny of the nascent HONO is dependent upon how the energy released in the primary decomposition of CH_2NNO_2 is distributed among the internal and translational modes of the fragments. Product energy averages for the diatomics resulting from HONO decomposition indicate that both HO and NO have little rotational excitation but substantial translational excitation.

Product energy distributions for reaction (I) are unremarkable. The translational energy distributions are peaked at small, nonzero energies (<9 kcal/mol) over the entire energy range and are similar to those calculated for simple bond scission reactions in other systems (see, for example, Sewell and Thompson 1991). Rotational energy distributions are also peaked at zero, indicating little rotational excitation.

It is difficult to apply the results of this study to the experimental measurements of Zhao, Hintsa, and Lee (1988), due to the uncertainty in the initial state of the nascent CH_2NNO_2 upon primary decomposition of RDX, and the ambiguity in the assignment of the parentage of the resulting final products. Based on these calculations and what is known about the PES, it seems reasonable to expect reaction (I) to play some role in the decomposition. However, Zhao, Hintsa, and Lee did not see

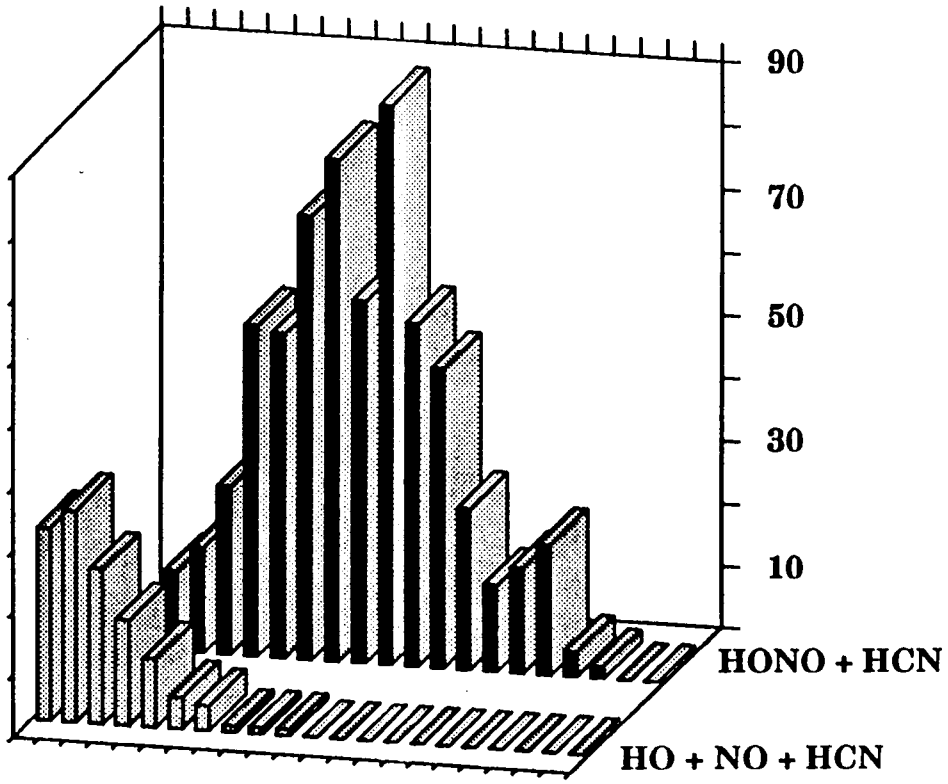

Figure 5. Relative translational energy distributions for HONO + HCN. Distribution with black bars correspond to HONO that do not undergo secondary decomposition and grey bars correspond to HONO that undergo N–O scission. Ticks along the abscissa are spaced 5 kcal/mol apart.

experimental evidence for this reaction (Zhao, Hintsa, and Lee 1988). Rather, the experiments have provided compelling evidence for the concerted reactions. The results of this study show that if sufficient energy is partitioned statistically among the internal modes of MN, then both reactions (I) and (II) will occur, with reaction (I) being more probable. Additionally, the decay curves, rate coefficients, and branching ratios show no anomalous behavior. One explanation that would satisfactorily explain the experimental result, without contradicting the simulation results, is that the internal energy of the nascent MN formed from primary decomposition of RDX is not distributed statistically in the molecule, but placed preferentially in vibrational modes that couple strongly into the concerted molecular elimination routes. We will pursue this possibility in a separate study.

5. SUMMARY

We have presented molecular dynamics simulations of the unimolecular decomposition of CH_2NNO_2. The potential energy function used in this study describes two competing reaction paths:

$$CH_2NNO_2 \rightarrow H_2CN + NO_2 \quad \text{(I)}$$

and

$$CH_2NNO_2 \rightarrow HCN + HONO. \quad \text{(II)}$$

The bond dissociation energy for N–N bond scission in (I) is 35 kcal/mol; this reaction has no back reaction barrier. The activation energy of (II) has been estimated to be 31 ± 4 kcal/mol based on the ab initio calculations (and corrections) by Mowrey et al. 1990. The transition state for this reaction is a five-centered cyclic structure with a classical barrier of 37 kcal/mol. The thermal activation energy for (II) is 31.8 kcal/mol.

Microcanonical rate coefficients were calculated by using classical trajectories at energies between 61 and 131 kcal/mol (including the zero-point energy, 27.5 kcal/mol). The results show that the dominant reaction path is (I), but at high energies (II) is competitive. The decay curves and corresponding branching ratios of the decomposition are linear and are well-described by the simple statistical RRK model (Robinson and Holbrook 1972). There does not appear to be an anomalous energy dependence of the rates of (I) and (II), as suggested in a previous study (Mowrey et al. 1990). HONO formed from (II) can undergo secondary reactions, including N–O bond scission, H–O bond scission, and hydrogen atom migration. The N–O scission and hydrogen atom migration appear to be energy dependent. The H–O scissions are infrequent events.

Product energy distributions for (I) are unremarkable and suggest that most energy available to the products remains in vibration. Product energy distributions for (II) are dependent on the fate of the HONO molecule. For the subset of HONO molecules that do not undergo decomposition, approximately 1/3 of the excess energy is deposited in relative translation between HONO and HCN, and approximately 50% in the vibrational modes. For the subset of HONO molecules that decompose to HO + NO, less than 10% of the excess energy is deposited in relative translation between HONO and HCN. Because the HCN rotational energy distributions do not differ between the two subsets, we conclude that HONO molecules that subsequently decompose have approximately 25% more energy partitioned into the vibrational modes upon CH_2NNO_2 decomposition than the HONO molecules that do not decompose.

Possible discrepancies between the simulations (which indicate that [I] is the major decomposition pathway) and experiment (which find concerted molecular elimination pathways to dominate) could be due to an anomalous energy distribution in the nascent CH_2NNO_2 upon RDX decomposition. We will investigate this possibility in another study.

INTENTIONALLY LEFT BLANK.

6. REFERENCES

Metropolis, N., A. W. Rosenbluth, M. N. Rosenbluth, A. H. Teller, and E. Teller. Journal of Chemical Physics, vol. 21, p. 1087, 1953.

Miller, W. H., and T. F. George. Journal of Chemical Physics, vol. 56, p. 5668, 1972.

Mowrey, R. C., M. Page, G. F. Adams, and B. H. Lengsfield, III. Journal of Chemical Physics, vol. 93, p. 1857, 1990.

Mowrey, R. C., M. Page, G. F. Adams, and B. H. Lengsfield, III. Unpublished.

Raff, L. M., and D. L. Thompson. Theory of Chemical Reaction Dynamics. Edited by M. Baer, vol. 4, Boca Raton, FL: CRC Press, 1985.

Rice, B. M., G. F. Adams, M. Page, and D. L. Thompson. "Analytical Potential Energy Surface for Methylene Nitramine (CH_2NNO_2)." U.S. Army Research Laboratory, Aberdeen Proving Ground, MD, to be published.

Robinson, P. J., and K. A. Holbrook. Unimolecular Reactions. New York: Wiley, 1972.

Schroeder, M. A. "Critical Analysis of Nitramine Decomposition Data: Product Distributions From HMX and RDX Decomposition." BRL-TR-2659, U.S. Army Ballistic Research Laboratory, Aberdeen Proving Ground, MD, June 1985a.

Schroeder, M. A. "Critical Analysis of Nitramine Decomposition Data: Activation Energies and Frequency Factors for HMX and RDX Decomposition." BRL-TR-2673, U.S. Army Ballistic Research Laboratory, Aberdeen Proving Ground, MD, June 1985b.

Sewell, T. D., and D. L. Thompson. Journal of Physical Chemistry, vol. 95, p. 6228, 1991.

Zhao, X., E. J. Hintsa, and Y. T. Lee. Journal of Chemical Physics, vol. 88, p. 801, 1988.

INTENTIONALLY LEFT BLANK.

NO. OF COPIES	ORGANIZATION
2	ADMINISTRATOR ATTN DTIC DDA DEFENSE TECHNICAL INFO CTR CAMERON STATION ALEXANDRIA VA 22304-6145
1	COMMANDER ATTN AMCAM US ARMY MATERIEL COMMAND 5001 EISENHOWER AVE ALEXANDRIA VA 22333-0001
1	DIRECTOR ATTN AMSRL OP SD TA US ARMY RESEARCH LAB 2800 POWDER MILL RD ADELPHI MD 20783-1145
3	DIRECTOR ATTN AMSRL OP SD TL US ARMY RESEARCH LAB 2800 POWDER MILL RD ADELPHI MD 20783-1145
1	DIRECTOR ATTN AMSRL OP SD TP US ARMY RESEARCH LAB 2800 POWDER MILL RD ADELPHI MD 20783-1145
2	COMMANDER ATTN SMCAR TDC US ARMY ARDEC PCTNY ARSNL NJ 07806-5000
1	DIRECTOR ATTN SMCAR CCB TL BENET LABORATORIES ARSENAL STREET WATERVLIET NY 12189-4050
1	DIR USA ADVANCED SYSTEMS ATTN AMSAT R NR MS 219 1 R&A OFC AMES RESEARCH CENTER MOFFETT FLD CA 94035-1000

NO. OF COPIES	ORGANIZATION
1	COMMANDER ATTN AMSMI RD CS R DOC US ARMY MISSILE COMMAND REDSTONE ARSNL AL 35898-5010
1	COMMANDER ATTN AMSTA JSK ARMOR ENG BR US ARMY TANK AUTOMOTIVE CMD WARREN MI 48397-5000
1	DIRECTOR ATTN ATRC WSR USA TRADOC ANALYSIS CMD WSMR NM 88002-5502
1	COMMANDANT ATTN ATSH CD SECURITY MGR US ARMY INFANTRY SCHOOL FT BENNING GA 31905-5660
	ABERDEEN PROVING GROUND
2	DIR USAMSAA ATTN AMXSY D AMXSY MP H COHEN
1	CDR USATECOM ATTN AMSTE TC
1	DIR USAERDEC ATTN SCBRD RT
1	CDR USACBDCOM ATTN AMSCB CII
1	DIR USARL ATTN AMSRL SL I
5	DIR USARL ATTN AMSRL OP AP L

INTENTIONALLY LEFT BLANK.

USER EVALUATION SHEET/CHANGE OF ADDRESS

This Laboratory undertakes a continuing effort to improve the quality of the reports it publishes. Your comments/answers to the items/questions below will aid us in our efforts.

1. ARL Report Number ARL-TR-691 Date of Report February 1995

2. Date Report Received _____

3. Does this report satisfy a need? (Comment on purpose, related project, or other area of interest for which the report will be used.) _____

4. Specifically, how is the report being used? (Information source, design data, procedure, source of ideas, etc.) _____

5. Has the information in this report led to any quantitative savings as far as man-hours or dollars saved, operating costs avoided, or effciencies achieved, etc? If so, please elaborate. _____

6. General Comments. What do you think should be changed to improve future reports? (Indicate changes to organization, technical content, format, etc.) _____

CURRENT ADDRESS

_____
Organization

_____
Name

_____
Street or P.O. Box No.

_____
City, State, Zip Code

7. If indicating a Change of Address or Address Correction, please provide the Current or Correct address above and the Old or Incorrect address below.

OLD ADDRESS

_____
Organization

_____
Name

_____
Street or P.O. Box No.

_____
City, State, Zip Code

(Remove this sheet, fold as indicated, tape closed, and mail.)

(DO NOT STAPLE)

DEPARTMENT OF THE ARMY

OFFICIAL BUSINESS

NO POSTAGE
NECESSARY
IF MAILED
IN THE
UNITED STATES

BUSINESS REPLY MAIL
FIRST CLASS PERMIT NO 0001, APG, MD

Postage will be paid by addressee

Director
U.S. Army Research Laboratory
ATTN: AMSRL-OP-AP-L
Aberdeen Proving Ground, MD 21005-5066